

# Hadron-gamma discrimination from an orbital UHECR observatory

A.D. Supanitsky\*, G. Medina-Tanco\*, K. Asano<sup>†</sup>, D. Cline<sup>§</sup>, T. Ebisuzaki<sup>¶</sup>,  
S. Inoue<sup>||</sup>, P. Lipari<sup>\*\*</sup>, N. Sakaki<sup>¶</sup>, A. Santangelo<sup>††</sup>, K. Shinozaki<sup>¶</sup>, G. Sigl<sup>‡‡</sup>, Y. Takahashi<sup>x</sup>  
and M. Teshima<sup>xi</sup> for the JEM-EUSO Collaboration

\* *Departamento de Física de Altas Energías, Instituto de Ciencias Nucleares, Universidad Nacional Autónoma de México, A. P. 70-543, 04510, México, D. F., México.*

<sup>†</sup> *Interactive Research Center of Science, Graduate School of Science, Tokyo Institute of Technology, 2-12-1 Ookayama Meguro-ku Tokyo 152-8550, Japan.*

<sup>§</sup> *Department of Physics and Astronomy, University of California, Los Angeles, USA.*

<sup>¶</sup> *RIKEN Advanced Science Institute, Japan.*

<sup>||</sup> *Dept. of Physics, Kyoto University, Kyoto 606-8502, Japan.*

<sup>\*\*</sup> *INFN-Roma La Sapienza, I-00185 Roma, Italy.*

<sup>††</sup> *Institute fuer Astronomie und Astrophysik Kepler Center for Astro and Particle Physics Eberhard Karls University Tuebingen Germany.*

<sup>‡‡</sup> *Institut theoretische Physik Universitaet Hamburg Luruper Chaussee 149 D-22761 Hamburg, Germany.*

<sup>x</sup> *Dept. of Physics, The University of Alabama in Huntsville, Huntsville, AL35899, USA.*

<sup>xi</sup> *Max-Planck-Institut für Physik, Föhringer Ring 6, D-80805 München, Germany.*

**Abstract.** The identification of very high energy photons is of great importance for the understanding of the origin of extreme energy cosmic rays (EECR). Several can be the sources of high energy photons at Earth. A guaranteed component is the flux of high energy photons expected as a consequence of the interaction of cosmic rays with the cosmic photon background. Another contribution may be expected as by-product at the acceleration sites of protons and nuclei, although such flux should be strongly suppressed for distant sources. On the other hand, top-down scenarios involving the decay of super heavy relic particles or topological defects, even if not currently favored, have as a characteristic signature an increasingly dominant flux of photons at the highest energies. In this work we study the statistical separation between hadron and photon showers at energies where both, LPM effect and magnetospheric interactions are important for the development of the cascades. We consider a detector with the same orbital characteristics as JEM-EUSO, but disregard trigger and reconstruction efficiencies, in order to define the maximum ideal discrimination power attainable.

**Keywords:** extreme-energy cosmic rays; photon fraction

## I. INTRODUCTION

The cosmic ray energy spectrum must have at least a minor component of ultra high energy photons. This component may receive contributions from different sources. Besides the expected flux generated by the propagation of the EECR in the intergalactic medium [1], photons may also be originated in different astrophysical environments as by-products of particle acceleration in

nearby cosmic ray sources (e.g. [2]) and, fundamentally, in top-down scenarios involving the decay of super heavy relic particles or topological defects [3]. Extreme energy photons have not been unambiguously observed yet. However, it is expected that JEM-EUSO [4], [5], with its unprecedented exposure will change this situation in the next few years.

In the present work we estimate the photon-proton discrimination power of JEM-EUSO. In particular we develop two complementary techniques to evaluate an upper limit on the fraction of photons relative to proton primaries in the integral cosmic rays flux by using the atmospheric depth of maximum development,  $X_{max}$ , of the corresponding atmospheric showers. The longitudinal evolution of high energy photon showers is dominated by the interplay between magnetospheric photon splitting and the LPM effect. The first process is highly dependent on the incoming direction of the photon with respect to the geomagnetic field and its intensity. Therefore, the translation of JEM-EUSO along its orbit is a distinctive parameter which adds richness and complexity to the analysis with respect to a traditional Earth bound observatory and must be taken into account.

## II. NUMERICAL APPROACH

Given a sample of  $N$  events, an ideal upper limit to the photon fraction may be calculated under the a priori assumption that actually no photon exists in the sample:

$$\mathcal{F}_\gamma^{min} = 1 - (1 - \alpha)^{1/N} \quad (1)$$

where  $\alpha$  is the confidence level of rejection. However, in practice, the probability of the existence of photons must be realistically assessed through some observational technique which involves the determination of

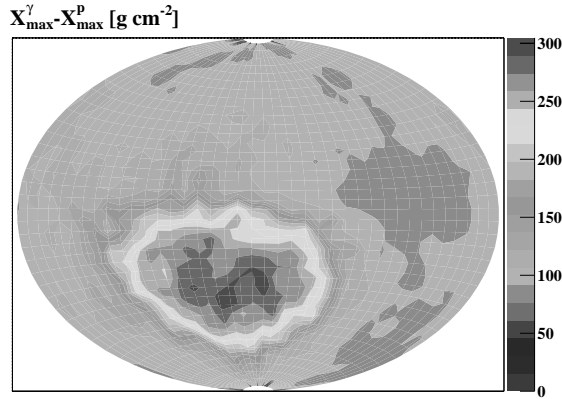


Fig. 1. Contour plot of  $X_{max}^{\gamma} - X_{max}^{pr}$  as a function of latitude and longitude in the Earth. The showers considered are such that  $\theta \in [30^{\circ}, 60^{\circ}]$  and  $E \in [10^{19.8}, 10^{20}]$  eV.

experimental parameters, which leads unavoidably to less restrictive upper limits than the previous one.

In this work the  $X_{max}$  parameter is considered for the discrimination of protons and photons showers. A shower library was generated by using the program CONEX [6] which consist of  $3 \times 10^5$  proton showers following a power law energy spectrum of spectral index  $\gamma = -2.7$  in the interval  $[10^{19.8}, 10^{21}]$  eV and with uniformly distributed arrival directions. Also  $> 5.1 \times 10^5$  photon showers were generated under the same conditions but in this case cores were also uniformly distributed on the surface of the Earth in order to properly take into account pre-showering (i.e., photon splitting) in the geomagnetic field.

A measure of the discrimination power of the  $X_{max}$  parameter is given by the merit factor,

$$\eta = \frac{\text{med}[X_{max}^{\gamma}] - \text{med}[X_{max}^{pr}]}{\sqrt{(\Delta X_{max}^{\gamma})^2 + (\Delta X_{max}^{pr})^2}} \quad (2)$$

where  $\text{med}[X_{max}^A]$  is the median of  $X_{max}^A$  ( $A = \gamma, pr$ ) distribution and  $\Delta X_{max}^A$  is one half of the length of the region of 68% of probability of  $X_{max}^A$  distribution.

Fig. 1 shows a contour plot of  $X_{max}^{\gamma} - X_{max}^{pr}$  as a function of latitude and longitude of the core on the Earth, for  $\theta \in [30^{\circ}, 60^{\circ}]$  and  $E \in [10^{19.8}, 10^{20}]$  eV. It can be seen that there are regions over the Earth surface where this difference is larger and in which the discrimination between protons and photons is more efficient.

Motivated by this result the concept of mask,  $\Omega(\eta_{Lim})$ , is introduced as those regions over the Earth surface where  $\eta$  is larger than a given value  $\eta_{Lim}$ . Fig. 2 shows the median of  $X_{max}$  and the region of 68% of probability as a function of primary energy for protons and photons with  $\theta \in [30^{\circ}, 60^{\circ}]$ . For the case of photons different masks are considered,  $\Omega(\eta_{Lim} = 0)$  (all events),  $\Omega(\eta_{Lim} = 1)$  and  $\Omega(\eta_{Lim} = 1.5)$ . Note that the masks are functions of primary energy. From the figure it can be seen that for the photons there are

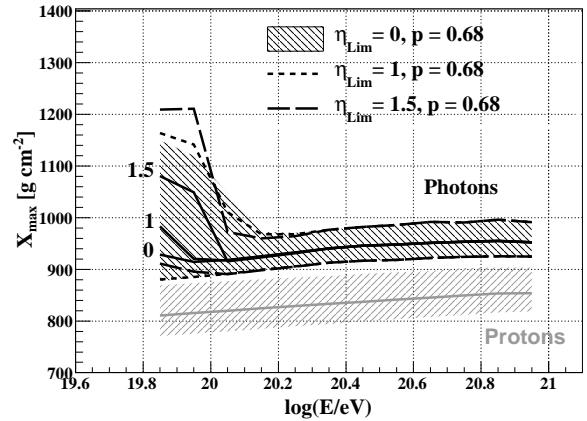


Fig. 2. Median and region of 68% of probability of  $X_{max}$  as a function of primary energy for  $\theta \in [30^{\circ}, 60^{\circ}]$ . In the case of photons different masks are considered,  $\eta_{Lim} = 0$  (all the events),  $\eta_{Lim} = 1$  and  $\eta_{Lim} = 1.5$ .

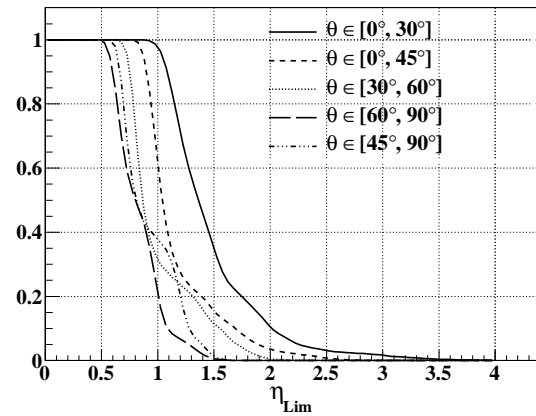


Fig. 3. Fraction of events as a function of  $\eta_{Lim}$  for different cuts in zenith angle and for  $E \in [10^{19.8}, 10^{20}]$  eV.

two well defined regions, the first corresponds to primary energies smaller than  $10^{20.1}$  eV in which the  $X_{max}^{\gamma}$  distribution is composed by LPM dominated showers that both, suffer and do not suffer photon splitting in the Earth magnetic field. In the second region all showers undergo photon splitting which generates, on average, smaller values of  $X_{max}^{\gamma}$  and smaller fluctuations [7].

The  $X_{max}^{\gamma}$  distributions obtained for masks with larger  $\eta_{Lim}$  allow a better separation between protons and photons. However, the total number of events also depends on the assumed mask and, in particular, decreases with  $\eta_{Lim}$ . Fig. 3 shows the fraction of events as a function of  $\eta_{Lim}$  for different cuts in zenith angle and for  $E \in [10^{19.8}, 10^{20}]$  eV. It can be seen that for vertical showers larger values of  $\eta$  are obtained which are also distributed over a wider range.

Two methods were developed in order to calculate an upper limit for the photon fraction. The first one is based

on the abundance estimator first introduced in [8],

$$\xi_{X_{max}} = \frac{1}{N} \sum_{i=0}^N \frac{f_{\gamma}(X_{max}^i)}{f_{\gamma}(X_{max}^i) + f_{pr}(X_{max}^i)} \quad (3)$$

where  $f_{\gamma}(X_{max})$  and  $f_{pr}(X_{max})$  are the photon and proton distribution functions,  $X_{max}^i$  are experimental values of  $X_{max}$  and  $N$  is the sample size.  $\xi_{X_{max}}$  is an estimator of the photon abundance,  $c_{\gamma} = N_{\gamma}/N$  where  $N_{\gamma}$  is the number of photons in the sample. The mean value of  $\xi_{X_{max}}$  is a linear function of  $c_{\gamma}$ , its standard deviation is proportional to  $1/\sqrt{N}$  and, for large values of  $N$ , it follows a Gaussian distribution.

For the case in which  $\xi_{X_{max}}$  is compatible with a pure proton sample, an upper limit to the photon fraction,  $c_{\gamma}^{min}$ , can be obtained from,

$$c_{\gamma}^{min} = \frac{4}{u_1^2} \left( \frac{u_1 \sqrt{v_2}}{\sqrt{N}} + \frac{v_1}{N} \right) \quad (4)$$

where  $u_1 = \alpha_1 - \alpha_2$ ,  $u_2 = \alpha_2$ ,  $v_1 = \alpha_3 - \alpha_4 + \alpha_2^2 - \alpha_1^2$  and  $v_2 = \alpha_4 - \alpha_2^2$ . Here

$$\alpha_1 = \int dX_{max} \frac{f_{\gamma}(X_{max})^2}{f_{\gamma}(X_{max}) + f_{pr}(X_{max})}, \quad (5)$$

$$\alpha_2 = \int dX_{max} \frac{f_{\gamma}(X_{max})f_{pr}(X_{max})}{f_{\gamma}(X_{max}) + f_{pr}(X_{max})}, \quad (6)$$

$$\alpha_3 = \int dX_{max} \frac{f_{\gamma}(X_{max})^3}{[f_{\gamma}(X_{max}) + f_{pr}(X_{max})]^2}, \quad (7)$$

$$\alpha_4 = \int dX_{max} \frac{f_{\gamma}(X_{max})^2 f_{pr}(X_{max})}{[f_{\gamma}(X_{max}) + f_{pr}(X_{max})]^2}. \quad (8)$$

The distribution functions needed to calculate  $c_{\gamma}^{min}$  are obtained from the simulated data by using the non-parametric method of kernel superposition with adaptive bandwidth [9].

It can be seen from Eq. (4) that, the larger the sample size, the smaller  $c_{\gamma}^{min}$ . Although, it is not obvious from this expression, it is possible to show that for larger values of  $\eta$  also smaller values of  $c_{\gamma}^{min}$  are obtained. Fig. 4 shows  $c_{\gamma}^{min}$  as a function of  $\eta_{Lim}$ , i.e. for different masks, for  $E \in [10^{19.8}, 10^{20}]$  eV,  $\theta \in [30^{\circ}, 60^{\circ}]$  and  $\theta \in [45^{\circ}, 90^{\circ}]$  and with and without assuming a Gaussian uncertainty of  $70 \text{ g cm}^{-2}$  for  $\theta \in [30^{\circ}, 60^{\circ}]$  and  $60 \text{ g cm}^{-2}$  for  $\theta \in [45^{\circ}, 90^{\circ}]$ . It can be seen that  $c_{\gamma}^{min}$  increases with  $\eta_{Lim}$ , which means that although the discriminator power of  $X_{max}$  increases the number of events decreases so rapidly producing larger values of  $c_{\gamma}^{min}$ , i.e. in this case the number of events is more important than the discrimination power of  $X_{max}$  for a given mask.

The second method developed here consists in finding a cut on  $X_{max}$  which minimizes the expression of the upper limit obtained assuming a pure proton composition,

$$\mathcal{F}_{UL}(X_{max}^c) = \frac{N_{\alpha}(NF_{pr}(X_{max}^c))}{NF_{\gamma}(X_{max}^c)}, \quad (9)$$

where  $N_{\alpha}(n)$  is the upper limit on the number of photons  $n$  at a confidence level  $\alpha$  obtained assuming

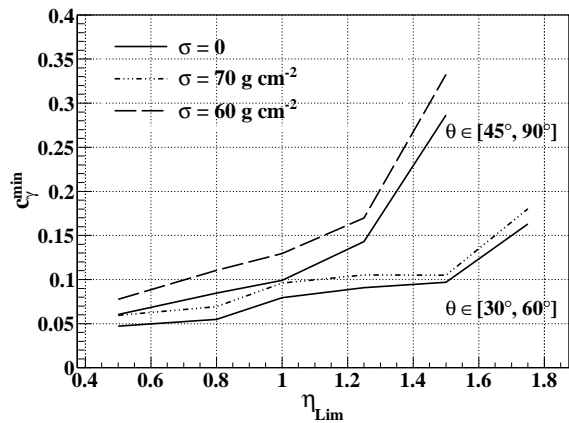


Fig. 4.  $c_{\gamma}^{min}$  as a function of  $\eta_{Lim}$  for  $E \in [10^{19.8}, 10^{20}]$  eV,  $\theta \in [30^{\circ}, 60^{\circ}]$  and  $\theta \in [45^{\circ}, 90^{\circ}]$  and with and without assuming a Gaussian uncertainty of  $70 \text{ g cm}^{-2}$  for  $\theta \in [30^{\circ}, 60^{\circ}]$  and  $60 \text{ g cm}^{-2}$  for  $\theta \in [45^{\circ}, 90^{\circ}]$ .

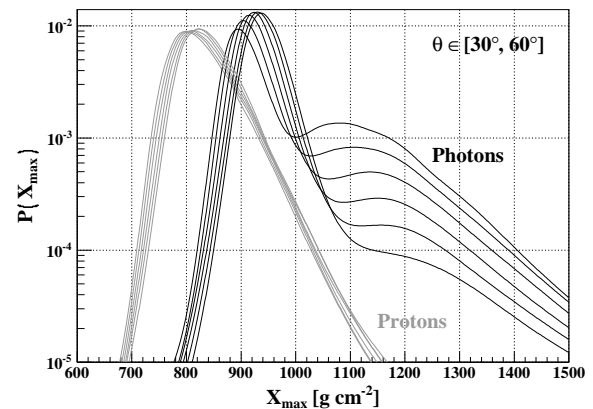


Fig. 5. Estimates of the protons and photons distribution functions of  $X_{max}$  for threshold energies from  $10^{19.8}$  eV to  $10^{20.3}$  eV in steps of  $\log(E/eV) = 0.1$  and for  $\theta \in [30^{\circ}, 60^{\circ}]$ . A power law energy spectrum of spectral index  $\gamma = -4.2$  is assumed. The mean value of the distributions increases with primary energy.

a Poisson distribution and

$$F_A(X_{max}^c) = \int_{X_{max}^c}^{\infty} dX_{max} f_A(X_{max}). \quad (10)$$

In order to study the upper limit for a given threshold energy the distribution functions of  $X_{max}$  for protons and photons are obtained from MC data, by using the non-parametric method of kernel superposition mentioned above. Fig. 5 shows the estimates of the proton and photon distribution functions for  $\theta \in [30^{\circ}, 60^{\circ}]$  and for threshold energies from  $10^{19.8}$  eV to  $10^{20.3}$  eV in steps of  $\log(E/eV) = 0.1$ . A power law energy spectrum of spectral index  $\gamma = -4.2$  following the shape of the Auger spectrum [10] is assumed. The figure shows, as expected, that as the threshold energy increases the bump due to the photons that do not suffer photon splitting in the geomagnetic field becomes progressively less important.

Fig. 6 shows  $\mathcal{F}_{UL}(X_{max}^c)$  as a function of  $X_{max}^c$

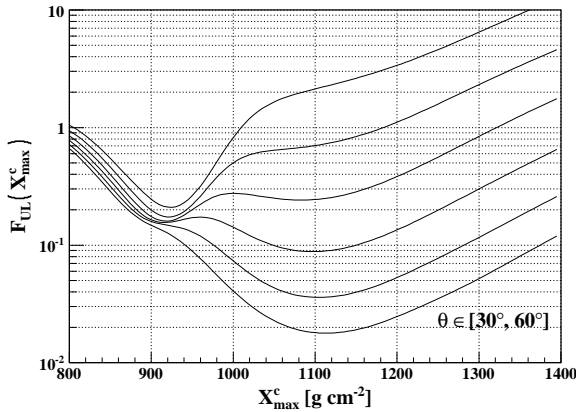


Fig. 6. Upper limit as a function of  $X_{max}^c$  for threshold energies from  $10^{19.8}$  eV to  $10^{20.3}$  eV in steps of  $\log(E/\text{eV}) = 0.1$  and for  $\theta \in [30^\circ, 60^\circ]$ .

obtained by using the distribution functions of Fig. 5, for  $\alpha = 0.95$  and for a total number of events above  $10^{19.8}$  eV  $N = 2250$  (4500 events in total but half of them have  $\theta \in [30^\circ, 60^\circ]$ ). It can be seen that  $\mathcal{F}_{UL}(X_{max}^c)$  reaches a minimum which depends on the threshold energy. Note that there is a transition at  $E_{th} = 10^{20}$  eV from which the minimum is reached at larger values of  $X_{max}^c$ . This is due to the change in the shape of the photon distribution function when the threshold energy increases (see Fig. 5). Finally, the upper limit is obtained evaluating  $\mathcal{F}_{UL}$  in  $X_{max}^c$  of the minimum.

Fig. 7 shows the upper limits on the fraction of photons in the integral cosmic ray flux, at 95% of confidence level, obtained in the ideal case  $\mathcal{F}_\gamma^{min}$  (dashed line), by using the  $\xi_{X_{max}}$  method for  $\theta \in [30^\circ, 60^\circ]$  and assuming a  $70 \text{ g cm}^{-2}$  of Gaussian uncertainty and no uncertainty in the determination of  $X_{max}$  (solid and dash-three dots-dash gray lines, respectively), by using the optimized cut method for  $\theta \in [30^\circ, 60^\circ]$  and assuming a 0 and  $70 \text{ g cm}^{-2}$  of Gaussian uncertainty in the determination of  $X_{max}$  (dash-dot-dash and solid black lines, respectively) and the upper limits obtained by different experiments. It can be seen that the upper limits obtained by using both methods introduced here are about one order of magnitude larger than the ideal case. This is due to the limitation imposed by the  $X_{max}$  parameter to discriminate between photons and protons. Moreover, for the energies  $> 10^{20}$  eV, the  $X_{max}$  distribution of photon showers is dominated by photon splitting decreasing the discrimination power of this parameter.

Fig. 7 also shows that for energies bellow  $10^{20.1}$  eV the optimized cut method results better than  $\xi_{X_{max}}$  method. This happens because the former takes advantage of the part of the distribution function originated by photons that do not suffer photon splitting. For larger energies the  $\xi_{X_{max}}$  method results better because the part of the  $X_{max}$  distribution of unconverted photons is less important and this methods takes into account the whole shape of proton and photon distribution functions.

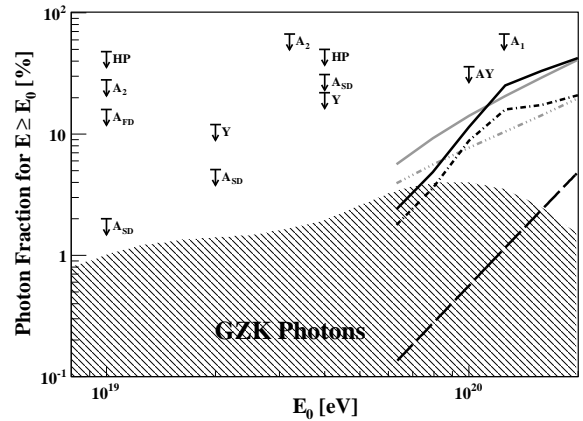


Fig. 7. The upper limits on the fraction of photons in the integral cosmic ray flux at 95% of confidence level. Dashed line corresponds to the ideal case in which it is known that there is no photons in the data. Solid and dash-three dots-dash gray lines are the upper limits obtained by using  $\xi_{X_{max}}$  method assuming a  $70 \text{ g cm}^{-2}$  of Gaussian uncertainty and no uncertainty in the determination of  $X_{max}$ , respectively. Solid and dash-dot-dash black lines are the upper limits obtained by using the optimized cut method assuming a  $0$  and  $70 \text{ g cm}^{-2}$  of Gaussian uncertainty in the determination of  $X_{max}$ , respectively. Shadow region is the prediction for the GZK photons [1]. Black arrows are experimental limits, HP: Haverah Park [11]; A<sub>1</sub>, A<sub>2</sub>: AGASA [12], [13]; A<sub>FD</sub>, A<sub>SD</sub>: Auger [14], [15]; AY: AGASA-Yakutsk [16]; Y: Yakutsk [17].

### III. CONCLUSIONS

In the present work we demonstrate that, based on pure statistics, JEM-EUSO will be able to set an upper limit to the photon fraction at the highest energies of  $\sim 10^{-1}$  %, well inside the GZK-photon flux expectation. A more realistic estimate, taking into account a conservative discrimination parameter and its experimental uncertainty the upper limit is larger but still considerably smaller than the corresponding values set so far by existing experiments. Therefore, given its large exposure, JEM-EUSO should be the first cosmic ray experiment to unambiguously detect cosmogenic photons.

### REFERENCES

- [1] G. Gelmini *et al.*, J. Exp. Theor. Phys. **106**, 1061 (2008).
- [2] M. Kachelriess, S. Ostapchenko, R. Tomas, arXiv:0805.2608.
- [3] R. Aloisio, V. Berezhinsky, M. Kachelriess, Phys. Rev. **D69**, 094023 (2004).
- [4] T. Ebisuzaki, 2009 *this proceedings*.
- [5] G. Medina-Tanco *et al.*, 2009 *this proceedings*.
- [6] T. Bergmann *et al.*, Astropart. Phys. **26**, 420 (2007).
- [7] H. Vankov *et al.*, Phys. Rev. **D67**, 043002 (2003).
- [8] A. D. Supanitsky, G. Medina-Tanco, A. Etchegoyen, Astropart. Phys. **31**, 75 (2008).
- [9] B. Silvermann, *Density Estimation for Statistics and Data Analysis*, Chapman and Hall, New York, 1986.
- [10] J. Abraham *et al.*, Phys. Rev. Lett. **101**, 061101 (2008).
- [11] M. Ave *et al.*, Phys. Rev. Lett. **85**, 2244 (2005). M. Ave *et al.*, Phys. Rev. **D65**, 063007 (2002).
- [12] M. Risse *et al.*, Phys. Rev. Lett. **95**, 171102 (2005).
- [13] K. Shinozaki *et al.*, Astrophys. J. **571**, L117 (2002).
- [14] J. Abraham *et al.*, Astropart. Phys. **27**, 155 (2007).
- [15] J. Abraham *et al.*, Astropart. Phys. **29**, 243 (2008).
- [16] G. Rubtsov *et al.*, Phys. Rev. **D73**, 063009 (2006).
- [17] A. Glushkov *et al.*, JETP Lett. **85**, 163 (2007).